

Geophysical Research Letters

RESEARCH LETTER

10.1029/2018GL079997

Key Points:

- A framework that computes the relative importance of the competing processes driving tropical cyclone rapid intensity changes is presented
- The relative roles of symmetric and asymmetric convection and other state variables within the vortex and in the environment are examined
- The most important generic markers that precede or lead to critical transitions in tropical cyclone intensity are objectively identified

Supporting Information:

- Supporting Information S1

Correspondence to:

S. Bhalachandran,
sbhalach@purdue.edu

Citation:

Bhalachandran, S., Haddad, Z. S., Hristova-Velva, S. M., & Marks, F. D. Jr. (2019). The relative importance of factors influencing tropical cyclone rapid intensity changes. *Geophysical Research Letters*, 46, 2282–2292. <https://doi.org/10.1029/2018GL079997>

Received 9 AUG 2018

Accepted 27 OCT 2018

Accepted article online 31 OCT 2018

Published online 21 FEB 2019

The Relative Importance of Factors Influencing Tropical Cyclone Rapid Intensity Changes

Saiprasanth Bhalachandran¹ , Ziad S. Haddad² , Svetla M. Hristova-Velva² , and F. D. Marks Jr.³ 

¹Department of Earth, Atmospheric, and Planetary Sciences, Purdue University, West Lafayette, IN, USA, ²Jet Propulsion Laboratory, California Institute of Technology, Pasadena, CA, USA, ³NOAA/AOML/Hurricane Research Division, Miami, FL, USA

Abstract Predicting rapid intensity changes in tropical cyclones (TCs) is a major challenge due to the influence of multiple competing processes within the vortex and in the TC environment. We present an empirical framework that quantifies the *relative importance* of the various factors that influence critical transitions in TC intensities. Our analysis of model simulations of recent TCs over the Bay of Bengal identifies the following variables *within the vortex* as the biggest influence on TC rapid intensity changes: the amplitudes of wave number 1 of 700- to 850-mb horizontal moisture flux convergence and precipitation in the rainband region and the amplitude of wave number 0 of precipitation within the radius of maximum winds. Likewise, the most important *environmental* variables identified are the angle between the driest air and the shear vector and the magnitude of vertical wind shear. These findings provide guidance on guidance for future observational efforts and data assimilation into TC forecasting models.

Plain Language Summary Critical transitions in tropical cyclone (TC) intensities are often very hard to predict because an intensity change is driven by multiple competing processes that act simultaneously in a complex and nonlinear fashion. To accurately forecast a TC's intensity evolution, it is very important to provide the best possible initial states to the forecast model. However, in reality, there are uncertainties in our knowledge of the initial state. This, coupled with the inherent nonlinearity in the system, makes it unwise to rely solely on deterministic forecasts. With this in mind, we derive empirical estimates of rapid intensification and weakening based on the current state of variables in the environment and in the vortex. Our framework identifies a set of *important* variables that are significantly different during time periods that just precede a rapid intensification as opposed to a rapid weakening. Our methodology then ranks the variables identified based on how their associated variability will be magnified over the course of model forecasts and how significantly they influence a rapid intensity change in a TC. The highest ranked variables must be prioritized in future observational and consequent modeling efforts that incorporate such observations as initial conditions of TC forecast models.

1. Introduction

A change in a tropical cyclone (TC)'s intensity is the manifestation of highly complex, nonlinear dynamical and thermodynamical processes interacting at and across multiple scales (Ooyama, 1982). These processes may be broadly classified as those intrinsic to a TC vortex and those external to it (Marks & Shay, 1998). The intrinsic processes range from aggregated and organized convective processes to those at disorganized cloud scales, to microphysical processes such as evaporation and precipitation (Montgomery & Smith, 2017). The processes external to a TC vortex are of much larger spatial and temporal scales (Hendricks et al., 2010; Raymond et al., 2015). Most importantly, the external and internal processes seek to act simultaneously, and the combined effect of these processes on a TC's intensity may be complementary, amplifying, inhibitive, or insignificant. For an accurate prediction of intensity (and intensity change), a mature understanding of the relative roles of the competing processes is crucial (Judt & Chen, 2016; Marks & Shay, 1998). The objective of the present study is to develop an empirical framework that can objectively quantify the relative roles of internal vortex variables versus external environmental variables in influencing a significant change in TC intensities.

Rapid intensity changes (RICs) in TCs are a special subset of the already baffling intensification problem where forecasting failures are more likely and can have dire consequences. In this study, we refer to RICs

(comprising rapid intensification, RI, and rapid weakening, RW) as an intensity change of ± 30 knots or greater in a span of 24 hr (Kaplan & DeMaria, 2003; Kotal & Roy Bhowmik, 2013; Wood & Ritchie, 2015). Due to the persistence and longer time scales associated with external, large-scale environmental processes, their roles in influencing RICs are better understood (Bhatia & Nolan, 2013; Emanuel et al., 2004; Judt et al., 2016; Kaplan & DeMaria, 2003; Kotal & Roy Bhowmik, 2013; Molinari et al., 1995; Molinari & Vollaro, 1989, 1990). Therefore, statistical indices targeted at RI prediction were developed primarily using large-scale environmental predictors (Kaplan & DeMaria, 2003; Kaplan et al., 2010; Rozoff et al., 2015). While there are no corresponding indices for RW over the ocean, empirical indices for rapid decay of TC intensity *post-landfall* have been developed (Kaplan & DeMaria, 1995). However, such indices have their limitations (Hendricks et al., 2010). Hendricks et al. cautioned that RI is mostly controlled by *internal dynamical processes* and therefore may not be well predicted by models that underrepresent such processes (see Text S1 in the supporting information).

In this light, only recently has the role of processes within the inner core of the vortex received sufficient attention from observational (Jiang, 2012; Kieper & Jiang, 2012; Rogers et al., 2013, 2016) and numerical (Chen & Gopalakrishnan, 2015; Leighton et al., 2018; Smith et al., 2017; Van Sang et al., 2008; Yang et al., 2007) efforts. The focus of these studies has largely been on the spatial (radial and azimuthal) distributions of symmetric and asymmetric convection. Their conclusions point to two distinct convective pathways that lead to RI: through asymmetric (isolated) bursts of intense convection or via well-organized, symmetric, albeit weaker convection. Here we take a holistic and objective perspective and address the relative importance of symmetric and asymmetric convective processes in causing RI or RW. Additionally, Rogers et al. (2013) noted that an important aspect that separated TCs that underwent RI from steady-state ones was the *radial* location of convection with respect to the radius of maximum winds (RMW). They found that during RI, the convection was located *inside* the RMW and, during other times, the convection was concentrated *outside* the RMW. Alternatively, other studies (Chen & Gopalakrishnan, 2015; Leighton et al., 2018; Rappin & Nolan, 2012) focus on the *azimuthal* distribution of convection with respect to the shear vector. However, these results are largely based on individual cases or idealized experiments, with very few systematic studies such as (Corbosiero & Molinari, 2003) conducted over a large number of cases that are sufficiently varied and representative to make statistically significant conclusions.

The present study aims to incorporate the insights from the above-mentioned studies and address the following specific scientific questions by analyzing a suite of TCs that experienced RICs: What is the relative importance of the following: (1) processes occurring at the vortex scale versus those occurring in the TC environment and (2) the spatial distribution of inner-core convection, specifically (a) the symmetric distribution versus asymmetric distribution of convection and (b) the radial distribution with respect to RMW versus the azimuthal distribution with respect to the shear vector.

It is important to note that any computation of the relative roles is useful only when you look at the behavior of a variable *in the context* of the other variables. For example, instead of questioning how important vortex-scale convective processes are for RIC, we seek to understand the importance of vortex-scale process in the context of multiple environmental backgrounds. To achieve our objectives, our empirical approach analyzes model simulations (details provided in the next section) of recent TCs that underwent RICs. Here we restrict our domain of study to the Bay of Bengal.

In addition to the complexity of the multiple processes interacting nonlinearly and acting simultaneously, there are uncertainties in the representations of these processes and in the initial conditions provided to our forecast models (Emanuel & Zhang, 2016; Rios-Berrios et al., 2014). The uncertainty in the knowledge of the initial values combined with the inherent stochasticity of processes we seek to simulate makes it unwise to rely solely on deterministic predictions (Judt et al., 2016; Zhang & Krishnamurti, 1999). With this in mind, we choose to focus on how the joint probability density functions of the initial values that evolve to rapidly intensify are different from those that evolve to rapidly weaken and what specifically about these initial values is different for the two populations. Kaplan et al. (2010) caution that the relative significance of various processes influencing a TC's intensity change may vary from basin to basin. From that perspective, the results and the subsequent interpretations presented here are directly linked to the basin of interest and the assumptions made in the model. However, our primary intent is to present a generic framework that allows for the quantification of the relative significance of the competing processes in a TC. We also seek to identify the *generic markers* or instantaneously measurable symptoms that indicate whether a TC is about to undergo RI or RW. Finally, we address how the variability of these markers affects the 24-hr change in the TC intensity; ENV = Environment.

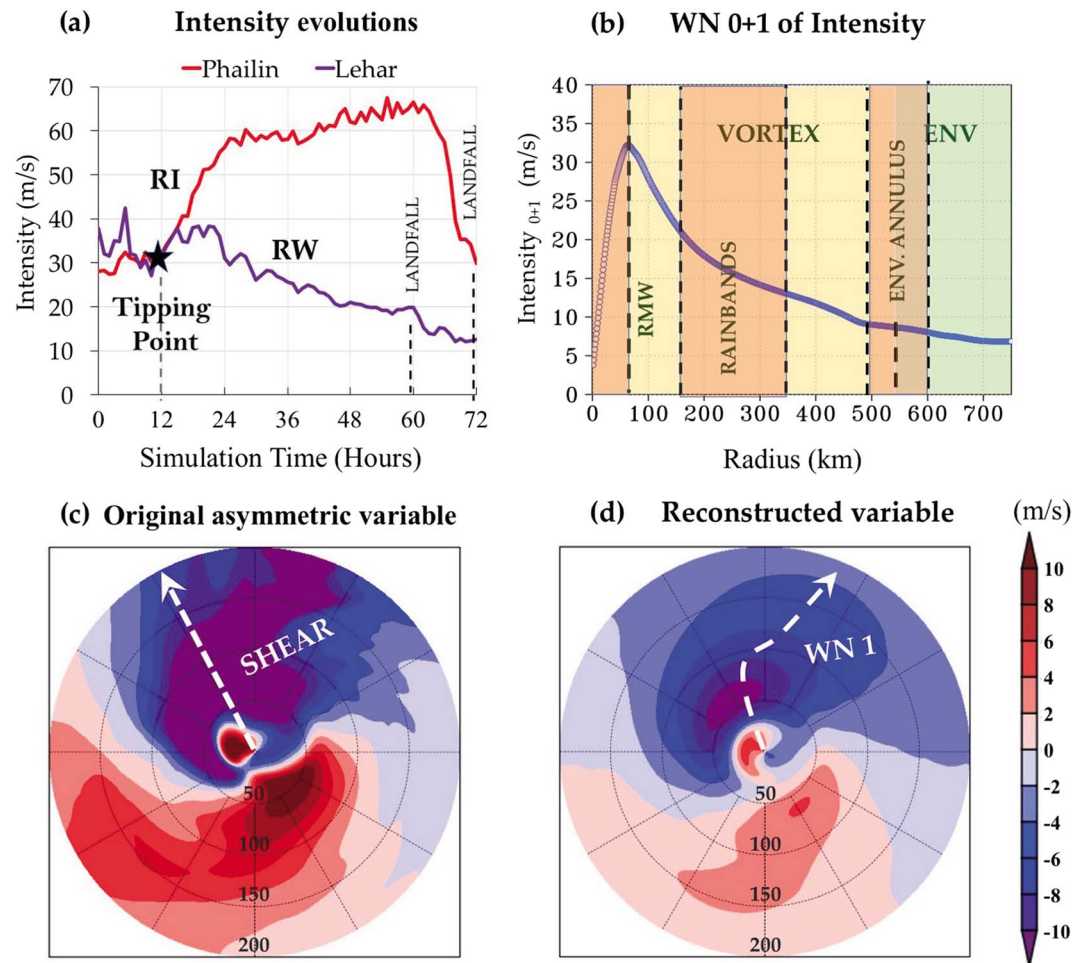


Figure 1. (a) Time series of intensity (maximum 10-m tangential winds) for TCs Phailin and Lehar forecast by the model. The rapid intensification phase of Phailin and the rapid weakening phase of Lehar are denoted as RI and RW, respectively. (b) Low WN reconstruction of TC Phailin's intensity at $t = 12$ (before the start of RI) used to identify the RMW, the rainband region, the bounds of the vortex, and the environmental annulus. (c) The horizontal cross section of Phailin's radial wind averaged between the surface and 850 mb represented in storm-centric, cylindrical coordinates. (d) Same as (c) except that the asymmetric variable is reduced to its lowest WN. The shear vector and the phase vector of WN 1 are highlighted. RI = rapid intensification; RMW = radius of maximum winds; RW = rapid weakening; TC = tropical cyclone; WN = wave number.

2. Data

TCs over the Bay of Bengal basin that experienced a RIC at least once over their life cycles between 2012 and 2017 are selected (Table S1). The Weather Research and Forecasting model (version 3.4.1) is used to simulate the above-mentioned TCs of interest, and the details of the model configurations are available in Table S2. These simulations use nested grids in which the grid spacing of the inner domain is 4 km and 1-hourly outputs are recorded. The simulations are then transformed to a storm-centric, cylindrical coordinate system where the center is defined as the minimum surface pressure centroid for each time. As an example, the time series of TC Phailin's and TC Lehar's intensities (maximum 10-m tangential wind in m/s) are shown in Figure 1a. Of interest here are the times just preceding a RIC (highlighted periods in Figure 1a). The TCs are not further classified based on their intensity, magnitude of shear, or proximity from land at the time of consideration. A total of 319 cases (158 RI and 151 RW) are obtained from these storms.

3. Low Wave Number Reconstruction

The following variables and combinations thereof from the WRF model outputs are initially selected to describe the instantaneous state of the vortex and the environment just before a RIC:

- Precipitation
- Radial and vertical component of wind
- Divergence of horizontal wind
- Relative humidity
- Environmental wind shear
- Horizontal moisture flux convergence

Note that this itself would amount to some 10^9 atmospheric state variables in the radial, azimuthal, and vertical dimensions over the domain. To reduce the dimensionality, these variables are first reduced to their wave numbers (WNs) 0 and 1 azimuthal harmonics (the lowest-order symmetric component, WN 0, and the lowest-order asymmetric component, WN 1) similar to the treatment in (Vukicevic et al., 2014) using the following equations:

$$f(r, \theta) \approx \hat{f}_0(r) + \hat{a}_1(r)\cos(\theta) + \hat{b}_1(r)\sin(\theta), \quad (1)$$

$$\text{where } \hat{f}_0(r) = \frac{1}{2\pi} \int_{-\pi}^{\pi} f(r, \theta) d\theta, \quad (2)$$

$$\hat{a}_1(r) = \frac{1}{2\pi} \int_{-\pi}^{\pi} f(r, \theta)\cos(\theta) d\theta, \quad (3)$$

$$\hat{b}_1(r) = \frac{1}{2\pi} \int_{-\pi}^{\pi} f(r, \theta)\sin(\theta) d\theta, \quad (4)$$

where $f(r, \theta)$ represents any 2D variable in a storm-centric, cylindrical coordinate framework; r and θ are the independent variables: radius and azimuthal angle, respectively; the hats indicate an azimuthal Fourier harmonic; and the subscript indicates which harmonic.

The low-WN reconstruction (WN 0 + 1) of 10-m tangential winds (intensity) of the individual cases was used to identify the radii corresponding to the maximum winds (RMW), the outer boundary of the vortex, and the environmental annulus as highlighted in Figure 1b. An example of how an original asymmetric variable (low-level radial wind) is reduced to its low-WN counterpart is depicted in Figures 1c and 1d. Also highlighted are the shear (defined as the vector difference between 200- and 850-mb averaged winds) vector in the original asymmetric variable and the WN 1 phase vector in the reconstructed variable. The outer boundary of the vortex is defined as the radius at which the WN 0 + 1 of intensity drops below 8 m/s. The environmental annulus is then defined as the annulus ± 50 km from the radius that marks the outer boundary of the vortex. Additionally, the radii between the 2*RMW and 5*RMW is denoted as the rainband region. Once these regions are defined for each case, the WN 0 and 1 coefficients of the variables listed above were obtained and then averaged over a handful of horizontal sectors (the disk within the RMW, the rainband annulus, and the environmental annulus) and four vertical layers (between 1,000 and 850 mb, 850 and 700 mb, 700 and 500 mb, and 350 and 200 mb). The subset of 26 variables listed in Table S3 was retained as the candidate variables whose relative importance in determining the 24-hr intensity change will be quantified (see Texts S2 and S3). We emphasize that this list was designed with a sole purpose to directly address the questions pertaining to the relative importance listed in section 1. As a result, this list of variables does not resemble the set of variables used previously to develop statistical RI indices (Kaplan & DeMaria, 2003; Kaplan et al., 2010; Kotal & Roy Bhowmik, 2013).

The assumption made here is that WN 1 represents most of the variance contained in the asymmetries (see Figure S1). Since the treatment of our problem of interest is that of an initial value problem, only the initial state at the beginning of the RIC period (and the boundary conditions) has any effect on the simulated TCs. From that perspective, all the effect from the higher order WNs (WNs 2 and higher) from previous times is already contained in the initial state. Such upscale and downscale exchanges between eddies of different WNs are detailed in Krishnamurti, et al. (2005). However, even if the higher order WNs are important to the evolution of the storm, WN 1 represents the organized asymmetries that are the most persistent in time and therefore have the best predictive potential (Vukicevic et al., 2014).

4. Computation of Linear Discriminants and Projection on to Principal Component Space

Given that we characterize an initial TC state with a small discrete set of variables x_1, x_2, \dots, x_n , the problem of separating points that were characterized as RI from points that are characterized as RW becomes one of finding

a hyperplane that separates the two sets of points in n -dimensional space. For two such objectively separated populations (RI and RW) with means $\vec{\mu}_{RI}$ and $\vec{\mu}_{RW}$, and with covariances C_{RI} and C_{RW} , the separation threshold (S) between the two distributions is defined as the ratio of the variances between the two populations to the variance within the populations (Fisher, 1936). The Fisher's linear discriminant is given by

$$[(C_{RI} + C_{RW})^{-1}(\vec{\mu}_{RI} - \vec{\mu}_{RW})^t] \vec{x} \geq [(C_{RI} + C_{RW})^{-1}(\vec{\mu}_{RI} - \vec{\mu}_{RW})^t] \frac{(\vec{\mu}_{RI} + \vec{\mu}_{RW})}{2}. \quad (5)$$

By denoting $[(C_{RI} + C_{RW})^{-1}(\vec{\mu}_{RI} - \vec{\mu}_{RW})^t]$ as α and the right-hand side as the threshold (S), this equation may be further written as

$$\alpha_1 \vec{x}_1 + \alpha_2 \vec{x}_2 + \dots + \alpha_n \vec{x}_n \geq S. \quad (6)$$

If the discriminant produced is greater than S , this means that \vec{x} leads to RI, and if the discriminant produced is less than S , it means that \vec{x} leads to RW.

After normalizing the variables \vec{x}_i by their respective variances, σ_i , equation (6) may be rewritten as:

$$\alpha_1 \sigma_1 \left(\frac{\vec{x}_1}{\sigma_1} \right) + \alpha_2 \sigma_2 \left(\frac{\vec{x}_2}{\sigma_2} \right) + \dots + \alpha_n \sigma_n \left(\frac{\vec{x}_n}{\sigma_n} \right) \geq S. \quad (7)$$

Consequently, $\alpha_1 \sigma_1 \dots \alpha_n \sigma_n$ are the coefficients (weights) associated with each of the normalized variables that may be compared. Note that the modeled cases are segmented into RI and RW a priori and that the variables associated with the biggest normalized weights in the linear discriminant analysis (LDA) are the most significant in causing the separation between the two populations.

Initially, no assumption is made about the relative importance of variables, and the entire list in Table S3 is subject to the LDA. The 319 cases are randomly split into one training and one testing subset following a 50:50 ratio, and the discriminant is computed. This exercise is repeated a thousand times while varying the training and testing data subsets. This randomization produces a thousand discriminants for a thousand subsamples. To decide whether the randomization of the training data set essentially produces the same discriminant for each of the 1,000 randomizations, or if instead it produces different discriminants that are highly dependent on the training set, the coefficients of the LDA resulting from each of the 1,000 iterations are projected onto their top two principal components (PCs). PC1 and PC2 capture most of the variability of these coefficients and, therefore, enable a two-dimensional quantification of their variability, as the training set is randomized (Figure 2a). Note how the variance is extremely high (order of magnitudes 10^6 and 10^7). Using the initial variable list, the LDA produced significantly different discriminants when the training data subsets were randomly varied. This is a clear evidence of overfitting. To rectify this, a novel technique was used, wherein we analyzed the coefficients of the discriminants for the cases that projected on the *extreme* ends in PC space, that is, around the edges of the ellipsoid capturing most of the points in PC1-PC2 space. By comparing the coefficients of the initial variable list for these cases, it was possible to identify the variables whose coefficients were consistent across different training sets and those whose coefficients exhibited a large variability, often changing signs while keeping relatively large magnitudes (See Text S4). An example of this is provided in Figures S2 and S3. The PC analysis revealed a core subset of variables whose coefficients were essentially constant regardless of the randomized training set used. These variables are listed in Figure 3a and Table S4. The 1,000 discriminants were rederived using this core subset, for each of the 1,000 randomized training sets. In this manner, we allowed the LDA to guide the set of variables to be used for analysis without making a subjective assumption regarding the relative importance of these variables. In the following section, only the LDA of the core subset of variables is presented. These 1,000 discriminants were then averaged, producing a single *mean* discriminant. The details on the selection of the optimal threshold (S) for the mean discriminant are provided in Figure S4.

5. Results of the Discriminant Analysis

Figure 4 presents the results of the LDA using only vortex-scale variables (Figure 4a), only the environmental variables (Figure 4b), and when all the variables are considered together (Figure 4c). The y-axis represents the magnitude of discriminant computed using the left-hand side of equation (7). The cases that underwent RI in reality are represented as blue, and those that underwent RW in reality are represented as red in Figure 4. Here

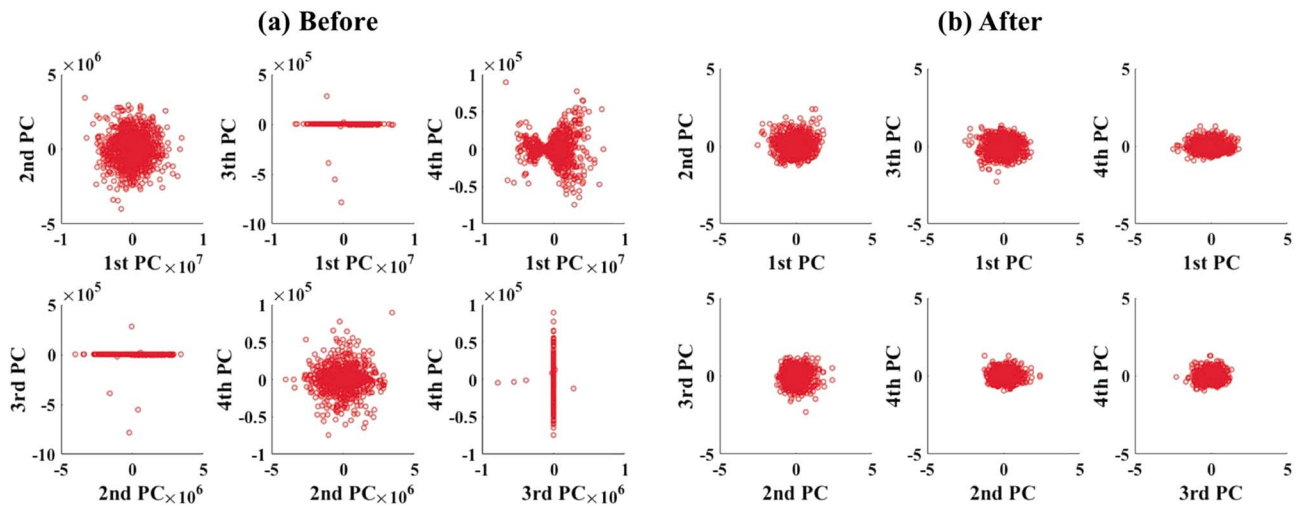


Figure 2. (a) Coefficients of the linear discriminant analysis performed iteratively using a 1,000 different training sets chosen from the superset of cases and the *initial* variable list projected on to principal component space. (b) Same as (a) but using only the consistent variables (after the removal of outliers). PC = principal component

a discriminant higher than the threshold (S) implies that the specific case is estimated by the LDA to undergo RI, and a discriminant less than S implies that the case is estimated by the LDA to undergo RW. Thus, the true positives, $pr(\text{estimated RI} | \text{true RI})$ in Figure 4, and true negatives, $pr(\text{estimated RW} | \text{true RW})$ in Figure 4, are indicated by blue lines with discriminants over S and red lines with discriminants less than S , respectively. Likewise, the false positives, $pr(\text{estimated RW} | \text{true RI})$ in Figure 4, and false negatives, $pr(\text{estimated RI} | \text{true RW})$ in Figure 4, are indicated by blue lines with discriminants less than S and red lines with discriminants greater than S . Note that the threshold (S) may be different in Figures 4a, 4b, and 4c.

Figure 4 demonstrates the following: (i) The discriminant computed with all the consistent set of variables taken together can effectively detect RI and RW with a high probability of detection and low probability of false alarm. (ii) Between the three scenarios presented in Figure 4, the best predictive capabilities are achieved by using a combination of vortex and environmental variables.

5.1. Generic Markers and Their Relative Importance

We refer to the core subset of the most consistent variables presented in Figure 3a as generic markers, since they are the best instantaneous *symptoms* of a forthcoming RIC. This section compares the relative importance of the different subsets among the consistent variables. Figure 3a shows the coefficients computed using the LDA corresponding to each variable, $w_n = \alpha_n \sigma_n$ as defined in equation (7). Figure 3a depicts the coefficients associated with the individual variables. Here the purple bars correspond to the scenario where all the variables are taken together, the golden bars correspond to the scenario where only the vortex variables are considered, and the green bars correspond to the scenario where only the environmental variables are considered for the LDA. At this juncture, it is important to note that the weights shown here are *in the context* of the other variables, hence the term *relative* importance. By themselves, the importance of the variables may not mean anything unless they are placed in the context of the other variables/processes acting simultaneously since the LDA relies on the separation between *joint* probability distributions of RI and RW populations. Due to this, the weight for the same variable may change when it is considered as part of the vortex variables alone and when it is considered as part of the entire list.

Figure 3a reveals that the most important vortex-scale variables are the amplitudes of the asymmetric fields (WN 1) of 850- to 700-mb horizontal moisture flux convergence, and WN 1 of rain in the rainband region, and the amplitude of the symmetric field (WN 0) of rain within the RMW. Likewise, the angle between the driest air and the shear vector and the magnitude of vertical wind shear are the most important environmental variables. The analysis also revealed that the sum of coefficients of all the environment variables compared to that of all the vortex variables (in the scenario where all of them were taken together) was 45:55. In other words, we can conclude that the environment and vortex variables are equally important (with a 5% error) in influencing a RIC.

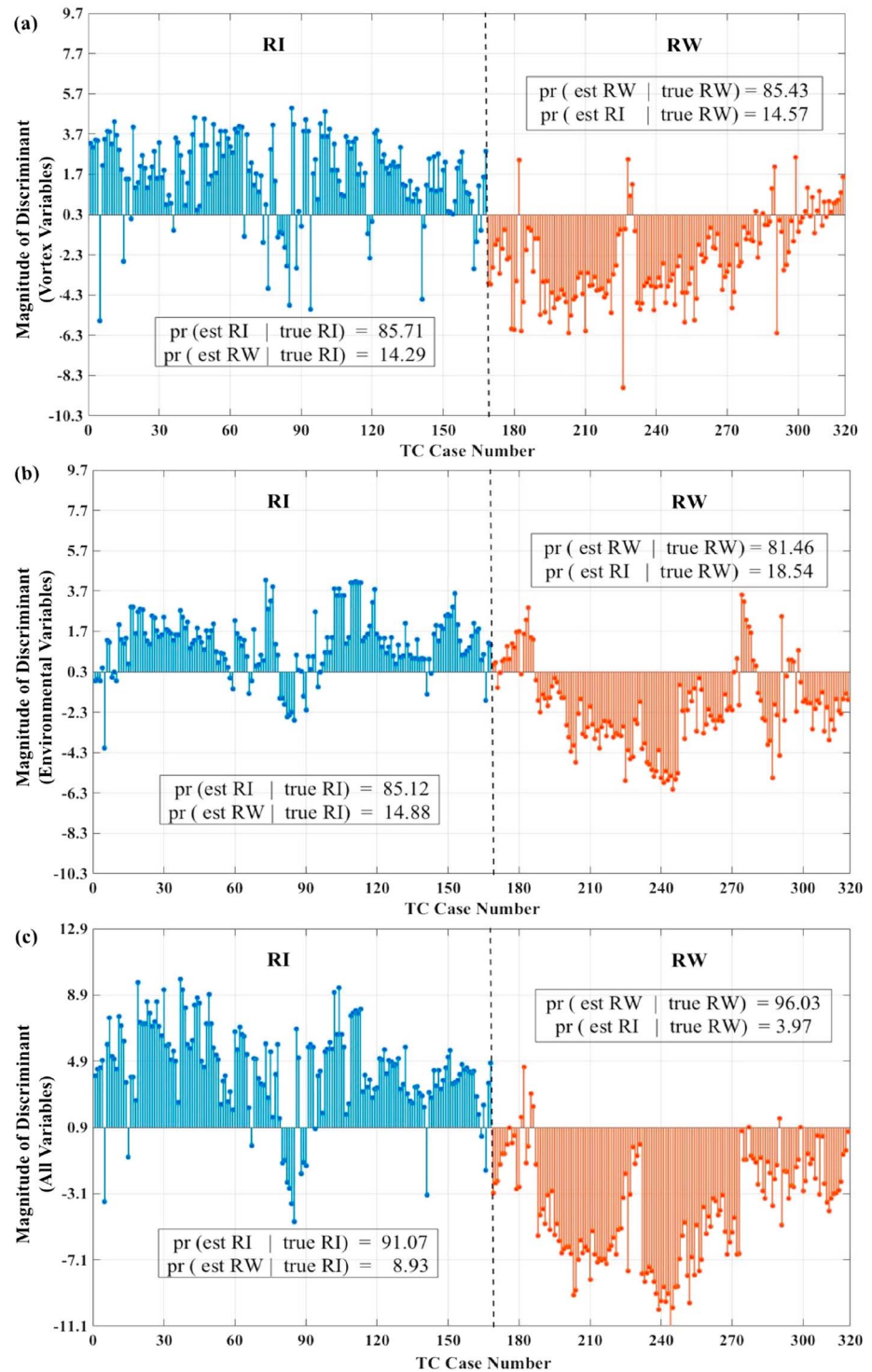


Figure 3. (a) Bar graph showing the weights (results of the LDA) that represent the relative importance of the environment and vortex variables. The purple bars show the results of the computation when all the variables are taken together; the golden bars show the results of LDA when only the vortex variables are taken together, and the green bars show the results of LDA when only the environment variables are taken together. (b) Same as (a) except that the bars indicate the results of LDA when only the precipitation variables within the vortex are considered. LDA = linear discriminant analysis; RMW = radius of maximum winds; WN = wave number.

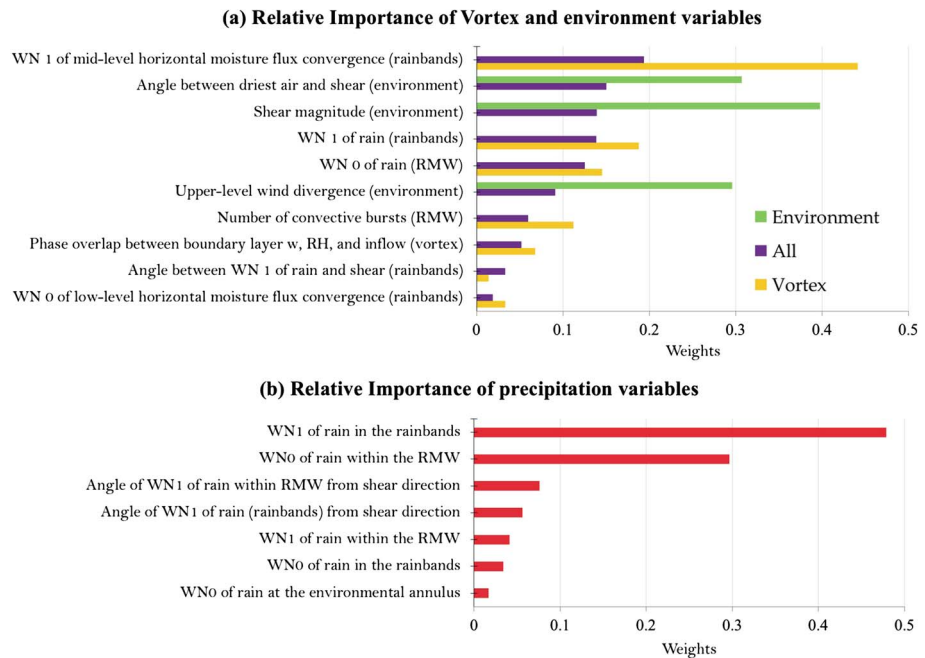


Figure 4. Results of the linear discriminant analysis. (a) Magnitude of discriminants computed for the RI and RW cases using only the vortex variables. (b) Same as (a) except that the computation is done only using the environmental variables. (c) Same as (a) except that the computation is done using both vortex and environmental variables together. The threshold (S) is marked by a horizontal line. Also highlighted are the estimated and true probabilities. RI = rapid intensification; RW = rapid weakening; TC = tropical cyclone.

Figure 3b shows the weights of the LDA computed with just the precipitation variables. Figure 3b reveals that the symmetric distribution of rain (WN 0) is most important within the RMW and that the asymmetric distribution (WN 1) is most important in the rain band region. Furthermore, Figure 3b indicates that the variables pertinent to the radial distribution of convection are more important than the azimuthal distribution with respect to the shear direction (both within the RMW and in the rain band region).

6. Discussions and Conclusions

The framework presented here offers a quantitative technique for testing the relative importance of the various external and internal processes influencing RICs in TCs over the Bay of Bengal. The assumption here is that the modeled cases are representative of the spectrum of TC behavior in the Bay of Bengal. At the core of this framework is the LDA that takes in inputs from modeled cases segmented into two populations—RI and RW. Such a scenario is akin to a steady-state TC with RI and RW as two distinct attractor basins. Given that there are multiple pathways for the TC to be pushed into one attractor or the other, the LDA identifies the variables that have the most significant impact on the TC evolution. To reduce the dimensionality associated with the variables required to describe the instantaneous state of the vortex and its environment, a low-WN reconstruction is performed before the LDA. The LDA then analyzes the joint probability distributions of the two populations and assigns coefficients based on how a particular variable affects the separation of the probability density functions in the two populations. The best separation of the two predicted populations is achieved using a combination of the vortex and environmental variables. The coefficients suggest that the aggregate contribution from the environmental variables and the vortex variables is nearly equal.

Our analysis of the relative roles of symmetric and asymmetric convective processes suggests that the vortex responds more markedly to the changes in the symmetric component (WN 0) of precipitation rather than the asymmetric, deep bursts of convection within the RMW. The greater the amplitude of WN 0 within the RMW, the more conducive is the configuration for the TC to undergo RI as opposed to RW. This finding is consistent with those of Gopalakrishnan et al. (2011), Kieper and Jiang (2012), and Rogers et al. (2016). It must be noted it is possible that an RI in its *initial* stage may be driven by asymmetric convection. Over time, as the RI continues, the convection may then wrap around in the azimuth, and the symmetric component may become dominant.

However, such a distinction cannot be made in the present study and will require a preclassification of the cases before the LDA. Outside the RMW, in the rainband region, the amplitudes of the asymmetric component (specifically WN 1 of precipitation and 850- to 700-mb horizontal moisture flux convergence) are seen to have a major influence. The manner in which the WN 1 of 850- to 700-mb (midlevel eddy flux) convergence of moisture acts to influence intensification or weakening is not straightforward to interpret. For example, the midlevel horizontal eddy moisture flux may act to bring in dry (moist) air into the storm core (Tang & Emanuel, 2010) and aid in the RW (intensification) of TCs. On the other hand, if the flux convergence of moist air occurs in the rainband region as opposed to the inner-core region, then these eddy fluxes may aid the growth of the rainband, thereby subtracting energy from the inner-core, and contribute to weakening. Likewise, the impact of WN 1 of precipitation in the rainband region on the TC undergoing RI/RW depends on the stage of the TC. If the TC is well developed, we speculate that the development of asymmetric precipitation in the rainband region will lead to weakening since the rainbands are subtracting energy from the TC core. On the other hand, in the early stages of the development of the TC, the asymmetric rain and convection in the rainband region may aggregate and advect radially inward into the core aiding in the intensification of the TC. Clearly, these topics require further investigation before we can arrive at definitive conclusions.

Furthermore, our results indicate that within the vortex, the amplitudes and radial location of asymmetric convection are more significant than the azimuthal phasing with respect to the shear in influencing a RIC. Again, the relative importance of the azimuthal distribution within the vortex might increase if the TCs are preclassified such that only those that experienced moderate to high environmental shear are considered. In the environmental annulus, the azimuthal phasing of the driest air is shown to be very important along with the magnitude of environmental shear. The impact of the magnitude of environmental vertical wind shear on TC intensity changes has been well documented (DeMaria, 1996; Frank & Ritchie, 2001; Riemer et al., 2010; Wong & Chan, 2004, and references therein). In summary, these studies suggest that low magnitudes of wind shear are expected to aid in the TC's intensification and high magnitudes are expected to aid in the TC's weakening. Moderate wind shear magnitudes are sources of high uncertainty, and either configuration is possible (Bhatia & Nolan, 2013; Rios-Berrios & Torn, 2017). Under such scenarios, the other external and intrinsic state variables are expected to dictate whether the TC will intensify or weaken. The alignment in the azimuthal phasing of the driest air with the shear vector will act to rapidly weaken the storm as evidenced by prior studies that have demonstrated the inhibitive role of dry air in the upshear quadrants (Leighton et al., 2018; Riemer et al., 2010; Rios-Berrios & Torn, 2017; Rogers et al., 2016).

Note that the identification of the *most important* markers does not imply that these are *sufficient* to predict the evolution of the TC. For example, when the LDA was performed with just the two variables with the highest weights, the predictive capabilities were significantly worse than those presented in Figure 4. This is because the variables with lesser weights help establish the context for the other variables to be more important. The correct way to interpret the coefficients is that they are weights in the sense that they magnify the effect of each variable. This means that if there is an uncertainty associated with these variables when they are fed in as inputs into a predictive model, their associated coefficients indicate how the uncertainty in those variables is magnified. From an observational perspective, we must know the markers with higher weights much better than the other, by a factor equal to the ratio of their coefficients. A detailed note on the satellite observations that may be used for estimating the highest ranked variables and the current gaps in our observations that limit their utility can be found in Text S5 (Arriaga, 2000; Aumann & Pagano, 1994; Bedka & Mecikalski, 2005; Draper et al., 2015; Figa-Saldaña et al., 2002; Hristova-Veleva et al., 2013; Kursinski et al., 1997; Randel & Park, 2006; Rodriguez & Hristova-Veleva, 2014; Spencer et al., 1994; Sun & Weng, 2008; Weng et al., 2012). We further recommend that the observations of the generic markers with the highest coefficients be assimilated as inputs into TC forecasting models for best predictive capabilities.

In the future, we seek to test the above methodology for not just instantaneous inputs, but *tendencies* of variables, and examine if that helps reduce uncertainty. Additionally, we intend to test the methodology using observations from satellites in addition to model outputs. By further separating the TC cases into subclasses based on (i) shear magnitude, (ii) intensity/stage of the vortex (e.g., nascent, developing, and mature), and (iii) proximity from land, it is possible to conduct the same analysis and see how the relative importance of the markers varied at different stages of a TC and for different classes of TCs. Furthermore, we seek to test the methodology for other basins such as the Atlantic and Pacific. An advancement of the technique used here would be an expanded representation of the problem nonlinearities, by including nonlinear transforms of

the initial state variables (such as the flux convergence of moisture or θ_e). These topics will be explored in a follow-up study.

Acknowledgments

The authors acknowledge WRF data provided by C-DAC Pune and the C-DAC National PARAM Supercomputing Facility. Majority of the work conducted here was performed during S. B's visit to the Jet Propulsion Laboratory, NASA, with financial support in the form of a NASA Earth Science Fellowship (Grant no: NNX15AM72H). The work of Z. S. Haddad and S. Hristova-Veleva was performed at the Jet Propulsion Laboratory, California Institute of Technology, under contract with NASA. The data and codes relevant to this manuscript are available here: https://drive.google.com/open?id=1Y_kFRfFc5IINPbfkuAB2qRe4TTXvjELA.

References

- Arriaga, A. (2000). Technical memorandum no. 5: Microwave humidity sounder (MHS) simulations with a radiative transfer model (EUMETSAT technical report).
- Aumann, H. H., & Pagano, R. J. (1994). Atmospheric infrared sounder on the earth observing system. *Optical Engineering*, 33(3), 776–785.
- Bedka, K. M., & Mecikalski, J. R. (2005). Application of satellite-derived atmospheric motion vectors for estimating mesoscale flows. *Journal of Applied Meteorology*, 44, 1761–1772.
- Bhatia, K. T., & Nolan, D. S. (2013). Relating the skill of tropical cyclone intensity forecasts to the synoptic environment. *Weather and Forecasting*, 28, 961–980.
- Chen, H., & Gopalakrishnan, S. G. (2015). A study on the asymmetric rapid intensification of hurricane earl (2010) using the HWRF system. *Journal of the Atmospheric Sciences*, 72, 531–550.
- Corbosiero, K. L., & Molinari, J. (2003). The relationship between storm motion, vertical wind shear, and convective asymmetries in tropical cyclones. *Journal of the Atmospheric Sciences*, 60(2), 366–376.
- DeMaria, M. (1996). The effect of vertical shear on tropical cyclone intensity change. *Journal of the atmospheric sciences*, 53(14), 2076–2088.
- Draper, D. W., Newell, D. A., Wentz, F. J., Krimchansky, S., & Skofronick-Jackson, G. M. (2015). The global precipitation measurement (GPM) microwave imager (GMI): Instrument overview and early on-orbit performance. *IEEE Journal of Selected Topics in Applied Earth Observations and Remote Sensing*, 8, 3452–3462.
- Emanuel, K., DesAutels, C., Holloway, C., & Korty, R. (2004). Environmental control of tropical cyclone intensity. *Journal of the Atmospheric Sciences*, 61, 843–858.
- Emanuel, K., & Zhang, F. (2016). On the predictability and error sources of tropical cyclone intensity forecasts. *Journal of the Atmospheric Sciences*, 73, 3739–3747.
- Figa-Saldaña, J., Wilson, J. J., Attema, E., Gelsthorpe, R., Drinkwater, M., & Stoffelen, A. (2002). The advanced scatterometer (ASCAT) on the meteorological operational (MetOp) platform: A follow on for european wind scatterometers. *Canadian Journal of Remote Sensing*, 28(3), 404–412.
- Fisher, R. A. (1936). The use of multiple measurements in taxonomic problems. *Annals of Eugenics*, 7(2), 179–188.
- Frank, W. M., & Ritchie, E. A. (2001). Effects of vertical wind shear on the intensity and structure of numerically simulated hurricanes. *Monthly Weather Review*, 129(9), 2249–2269.
- Gopalakrishnan, S. G., Marks, F. Jr., Zhang, X., Bao, J.-W., Yeh, K.-S., & Atlas, R. (2011). The experimental HWRF system: A study on the influence of horizontal resolution on the structure and intensity changes in tropical cyclones using an idealized framework. *Monthly Weather Review*, 139, 1762–1784.
- Hendricks, E. A., Peng, M. S., Fu, B., & Li, T. (2010). Quantifying environmental control on tropical cyclone intensity change. *Monthly Weather Review*, 138, 3243–3271.
- Hristova-Veleva, S. M., Callahan, P. S., Dunbar, R. S., Stiles, B. W., Yueh, S. H., Huddleston, J. N., et al. (2013). Revealing the winds under the rain. part i: Passive microwave rain retrievals using a new observation-based parameterization of subsatellite rain variability and intensity algorithm description. *Journal of Applied Meteorology and Climatology*, 52, 2828–2848.
- Jiang, H. (2012). The relationship between tropical cyclone intensity change and the strength of inner-core convection. *Monthly Weather Review*, 140, 1164–1176.
- Judt, F., & Chen, S. S. (2016). Predictability and dynamics of tropical cyclone rapid intensification deduced from high-resolution stochastic ensembles. *Monthly Weather Review*, 144, 4395–4420.
- Judt, F., Chen, S. S., & Berner, J. (2016). Predictability of tropical cyclone intensity: Scale-dependent forecast error growth in high-resolution stochastic kinetic-energy backscatter ensembles. *Quarterly Journal of the Royal Meteorological Society*, 142, 43–57.
- Kaplan, J., & DeMaria, M. (1995). A simple empirical model for predicting the decay of tropical cyclone winds after landfall. *Journal of Applied Meteorology*, 34(11), 2499–2512.
- Kaplan, J., & DeMaria, M. (2003). Large-scale characteristics of rapidly intensifying tropical cyclones in the North Atlantic Basin. *Weather and Forecasting*, 18(6), 1093–1108.
- Kaplan, J., DeMaria, M., & Knaff, J. A. (2010). A revised tropical cyclone rapid intensification index for the Atlantic and eastern North Pacific basins. *Weather and Forecasting*, 25, 220–241.
- Kieper, M. E., & Jiang, H. (2012). Predicting tropical cyclone rapid intensification using the 37 GHz ring pattern identified from passive microwave measurements. *Geophysical Research Letters*, 39, L13804. <https://doi.org/10.1029/2012GL052115>
- Kotal, S. D., & Roy Bhowmik, S. K. (2013). Large-scale characteristics of rapidly intensifying tropical cyclones over the Bay of Bengal and a rapid intensification (RI) index. *Mausam*, 64(1), 13–24.
- Krishnamurti, T. N., Pattnaik, S., Stefanova, L., Kumar, T. V., Mackey, B. P., O'Shay, A. J., & Pasch, R. J. (2005). The hurricane intensity issue. *Monthly Weather Review*, 133(7), 1886–1912. <https://doi.org/10.1175/MWR2954.1>
- Kursinski, E., Hajj, G., Schofield, J., Linfield, R., & Hardy, K. R. (1997). Observing Earth's atmosphere with radio occultation measurements using the global positioning system. *Journal of Geophysical Research*, 102(D19), 23,429–23,465.
- Leighton, H., Gopalakrishnan, S., Zhang, J. A., Rogers, R. F., Zhang, Z., & Tallapragada, V. (2018). Azimuthal distribution of deep convection, environmental factors, and tropical cyclone rapid intensification: A perspective from HWRF ensemble forecasts of hurricane Edouard (2014). *Journal of the Atmospheric Sciences*, 75, 275–295.
- Marks, F. D., & Shay, L. K. (1998). Landfalling tropical cyclones: Forecast problems and associated research opportunities. *Bulletin of the American Meteorological Society*, 79(2), 305–323.
- Molinari, J., Skubis, S., & Vollaro, D. (1995). External influences on hurricane intensity. part iii: Potential vorticity structure. *Journal of the Atmospheric Sciences*, 52(20), 3593–3606.
- Molinari, J., & Vollaro, D. (1989). External influences on hurricane intensity. part i: Outflow layer eddy angular momentum fluxes. *Journal of the Atmospheric Sciences*, 46(8), 1093–1105.
- Molinari, J., & Vollaro, D. (1990). External influences on hurricane intensity. part ii: Vertical structure and response of the hurricane vortex. *Journal of the Atmospheric Sciences*, 47(15), 1902–1918.
- Montgomery, M. T., & Smith, R. K. (2017). Recent developments in the fluid dynamics of tropical cyclones. *Annual Review of Fluid Mechanics*, 49, 541–574.
- Ooyama, K. V. (1982). Conceptual evolution of the theory and modeling of the tropical cyclone. *Journal of the Meteorological Society of Japan. Ser. II*, 60(1), 369–380.

- Randel, W. J., & Park, M. (2006). Deep convective influence on the Asian summer monsoon anticyclone and associated tracer variability observed with atmospheric infrared sounder (AIRS). *Journal of Geophysical Research*, *111*, D12314.
- Rappin, E. D., & Nolan, D. S. (2012). The effect of vertical shear orientation on tropical cyclogenesis. *Quarterly Journal of the Royal Meteorological Society*, *138*, 1035–1054.
- Raymond, D., Fuchs, Z., Gjorgjievska, S., & Sessions, S. (2015). Balanced dynamics and convection in the tropical troposphere. *Journal of Advances in Modeling Earth Systems*, *7*, 1093–1116.
- Riemer, M., Montgomery, M. T., & Nicholls, M. E. (2010). A new paradigm for intensity modification of tropical cyclones: Thermodynamic impact of vertical wind shear on the inflow layer. *Atmospheric Chemistry & Physics*, *10*, 3163–3188.
- Rios-Berrios, R., & Torn, R. D. (2017). Climatological analysis of tropical cyclone intensity changes under moderate vertical wind shear. *Monthly Weather Review*, *145*, 1717–1738.
- Rios-Berrios, R., Vukicevic, T., & Tang, B. (2014). Adopting model uncertainties for tropical cyclone intensity prediction. *Monthly Weather Review*, *142*, 72–78.
- Rodriguez, E., & Hristova-Veleva, S. (2014). Multidecadal consistent ocean vector winds: From QuikSCAT to RapidSCAT and beyond. American Geophysical Union, Fall Meeting 2014, Abstract O551D-01.
- Rogers, R., Reasor, P., & Lorsolo, S. (2013). Airborne Doppler observations of the inner-core structural differences between intensifying and steady-state tropical cyclones. *Monthly Weather Review*, *141*, 2970–2991.
- Rogers, R., Zhang, J. A., Zawislak, J., Jiang, H., Alvey, G. R. III, Zipser, E. J., & Stevenson, S. N. (2016). Observations of the structure and evolution of Hurricane Edouard (2014) during intensity change. Part II: Kinematic structure and the distribution of deep convection. *Monthly Weather Review*, *144*, 3355–3376.
- Rozoff, C. M., Velden, C. S., Kaplan, J., Kossin, J. P., & Wimmers, A. J. (2015). Improvements in the probabilistic prediction of tropical cyclone rapid intensification with passive microwave observations. *Weather and Forecasting*, *30*, 1016–1038.
- Smith, R. K., Zhang, J. A., & Montgomery, M. T. (2017). The dynamics of intensification in a hurricane weather research and forecasting simulation of Hurricane Earl (2010). *Quarterly Journal of the Royal Meteorological Society*, *143*, 293–308.
- Spencer, R. W., Hood, R. E., Lafontaine, F. J., Smith, E. A., Platt, R., Galliano, J., et al. (1994). High-resolution imaging of rain systems with the advanced microwave precipitation radiometer. *Journal of Atmospheric and Oceanic Technology*, *11*(4), 849–857.
- Sun, N., & Weng, F. (2008). Evaluation of special sensor microwave imager/sounder (SSMIS) environmental data records. *IEEE Transactions on Geoscience and Remote Sensing*, *46*, 1006–1016.
- Tang, B., & Emanuel, K. (2010). Midlevel ventilations constraint on tropical cyclone intensity. *Journal of the Atmospheric Sciences*, *67*, 1817–1830.
- Van Sang, N., Smith, R. K., & Montgomery, M. T. (2008). Tropical-cyclone intensification and predictability in three dimensions. *Quarterly Journal of the Royal Meteorological Society*, *134*, 563–582.
- Vukicevic, T., Uhlhorn, E., Reasor, P., & Klotz, B. (2014). A novel multiscale intensity metric for evaluation of tropical cyclone intensity forecasts. *Journal of the Atmospheric Sciences*, *71*, 1292–1304.
- Weng, F., Zou, X., Wang, X., Yang, S., & Goldberg, M. D. (2012). Introduction to Suomi National Polar-orbiting Partnership advanced technology microwave sounder for numerical weather prediction and tropical cyclone applications. *Journal of Geophysical Research*, *117*, D19112.
- Wong, M. L., & Chan, J. C. (2004). Tropical cyclone intensity in vertical wind shear. *Journal of the Atmospheric Sciences*, *61*, 1859–1876.
- Wood, K. M., & Ritchie, E. A. (2015). A definition for rapid weakening of North Atlantic and eastern North Pacific tropical cyclones. *Geophysical Research Letters*, *42*, 10–091.
- Yang, B., Wang, Y., & Wang, B. (2007). The effect of internally generated inner-core asymmetries on tropical cyclone potential intensity. *Journal of the Atmospheric Sciences*, *64*, 1165–1188.
- Zhang, Z., & Krishnamurti, T. (1999). A perturbation method for hurricane ensemble predictions. *Monthly Weather Review*, *127*(4), 447–469.